Measurements of Doppler and delay spreading of communication signals in medium depth and shallow underwater acoustic channels

Michael Caley (1), Dr Alec Duncan (1), Allesandro Ghiotto(2)

(1) Curtin University, Centre for Marine Science and Technology, Perth, Australia

(2) L3-Communications Nautronix Ltd, Fremantle, Australia

ABSTRACT

Recent measurements of Doppler and delay spreading of underwater acoustic communication signals are presented for 84m and 14m deep marine environments off the coast of Perth, Western Australia. The data-sets are being utilised to develop a computer model of the transient Doppler and delay spreading effects of surface waves. The work supports the on-going development of a dynamic underwater acoustic communication channel simulator to assist the testing of modems and signalling strategies in varied conditions in a cost-effective manner.

INTRODUCTION

Most if not all practical underwater communication channels are significantly dynamic due to one or more of the following time-variant aspects: transmitter and or receiver movement; moving sea surface; surface-bubble entrainment, variable ambient noise, and time-varying sound speed profiles. These factors produce a continuously varying channel impulse response and associated frequency domain effects such as Doppler shifts and Doppler spreading.

Simulation of the response of an underwater acoustic communication channel and associated ambient noise assists the development of signal encoding and demodulation systems in a cost-effective and controlled manner, however the success of the simulation is dependent on the simulator being able to reproduce the significant fine time-scale response characteristics of the channel that challenge the performance of underwater communication systems (Karasalo, 2011, Socheleau et al., 2011, Freitag et al., 2001).

The reported characteristics of the underwater channel that are key to the development of an acoustic channel simulator for high-rate data communications are the transient delay and Doppler spreading imparted by the moving sea-surface (Eggen, 2001), and the transient Doppler imparted by moving transmitter and or receiver platforms (van Walree et al., 2008).

CHANNEL PROBING EXPERIMENTS

Channel probing experiments have been conducted to explore the transient impulse response characteristics of shallow and medium depth ocean channels near Perth. The experiments have been conducted to assist in the development of a dynamic underwater acoustic communication channel simulator.

A shallow water channel probing experiment was conducted in April 2012 near to the Cottesloe Directional Wave Rider Buoy in a water depth of 13m to 14m, over distances of 50m to 1000m. The transmitter and receiver arrangements are illustrated in Figure 1 and Figure 2. The transmitter was inverted to maximise the signal directivity for surface reflected transmission paths.

Opportunistic channel probing in conjunction with an L3-Nautronix hardware deployment was conducted in March 2012 in mid-depth (84m) waters off Rottnest Island over similar distances. This test involved the sampling of low-frequency acoustic array alignment signals in addition to short duration communication signals. The transmitter and receiver setups were similar to Figure 1 but with the transmitter oriented with its maximum response directed downwards as required by the primary purpose of the transmissions. The receiver arrangement was similar to Figure 2 but utilising an acoustic release for recovery and without the temperature loggers in the water column.

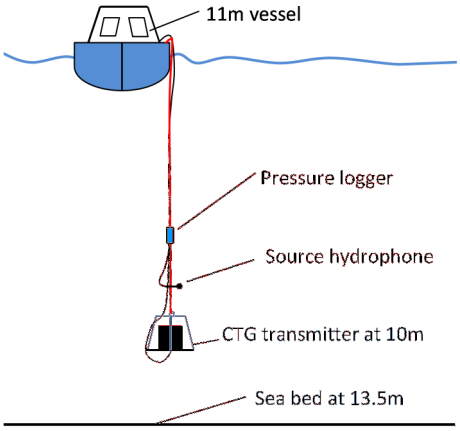

Figure 1. Shallow channel transmitter

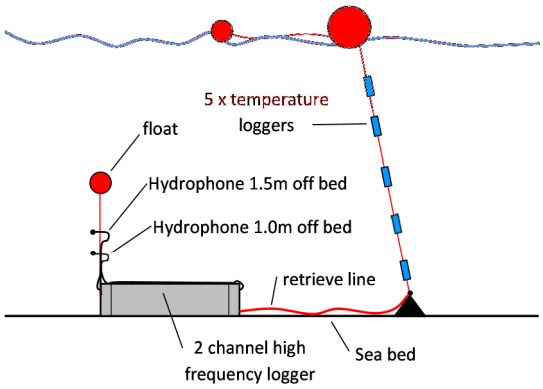

Figure 2. Shallow channel receiver

Experimental arrangement and instrumentation

Consideration was given to the merits of fixed versus variable transmitter/receiver motion before opting for a moving transmitter platform. Fixed transmitter and receiver positions enable the Doppler effects of the channel to be experimentally isolated (van Walree et al., 2010), however the flexibility in exploring different ranges and transmit angles relative to prevailing surface wave directions would be limited. A moving transmitter introduces additional complexity to the task of separating platform movement transient effects from channel transient effects, but achieves greater flexibility and generality in the resultant data analysis.

The acoustic receiver logger recorded two hydrophones separated vertically by 0.5m to explore the benefit of spatial diversity to counteract transient modal nulls at the receiver. The separation was selected based on fine-resolution Belhop(Porter, 2011) TL simulations within the 9kHz to 15kHz experimental signal bandwidth.

Transmitted and received signals were sampled with 24 bit resolution at 96 kHz. Directional surface wave data was obtained for the Cottesloe Directional Wave Rider Buoy (DWRB) and the Rottnest Island DWRB. The sound-speed profile at each site was sampled with a Conductivity Temperature Depth (CTD) probe. The GPS position was logged at 1s intervals. A pressure transducer sampling at 8Hz was attached to the transmitter.

For the shallow channel experiment a number of additional sampling systems were utilised. The vessel was fitted with pitch, heave and roll data acquisition sampling at 100 kHz, and five temperature loggers sampling at 60 second intervals were suspended from the surface float line. Grab samples of the bottom material were collected.

Probe signals

The channel impulse response exhibits transient effects on multiple time-scales including hours for sound speed structure (Siderius et al., 2007), the timescale of swell periods, which can be up to 20s, and finer timescales of the order of milliseconds associated with transient surface reflected soundpaths (Stojanovic and Preisig, 2009).

A selection of probe signal sequence lengths and waveforms were transmitted to explore delay and Doppler effects on different time scales as summarised in Table 1 and Table 2.

For the shallow trial, fine scale temporal effects were explored by repeating a short duration bipolar pseudorandom number (PN) sequence modulating a 12kHz continuous wave (CW) carrier, and a 16ms frequency sweep, providing high resolution of delay information when the source and received signal are cross-correlated. The longer temporal effects associated with wave and swell were explored by continuing the repetitions over an interval greater than the wave period. A repeated pattern was transmitted of 60s of n=4095, 30s of n=511 and 30s of n=63, where n is the number of stages or chips in the PN sequence. This was followed by 60 s of simultaneous stacked CWs, then 30 repeats of a 16ms 8kHz-16kHz frequency sweep at 1s intervals. The, modulated bandwidth, duration and sound pressure level of this repeated pattern of signals is illustrated in Figure 3 and Figure 4.

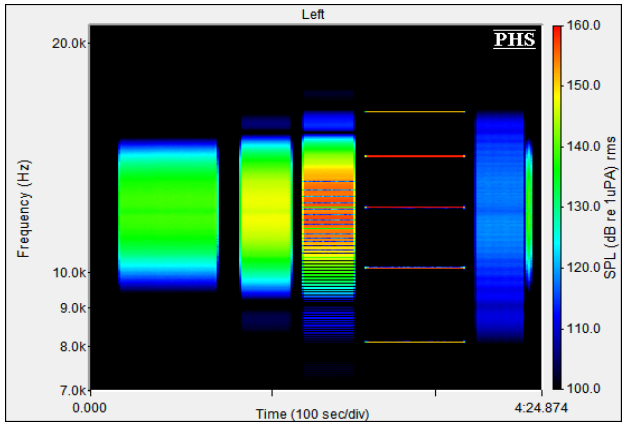

Figure 3. Probe signal spectra – shallow trial

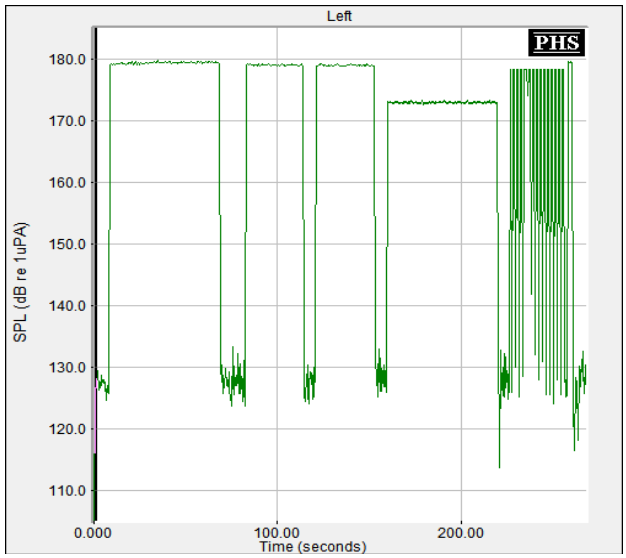

Figure 4. Probe signal levels at 1m- shallow trial

Table 1. Shallow trial test signals

Signal	Carrier F_o (kHz)	repeat period, T (s)	Band-width, B (Hz)	Delay Res. (ms)	Dopp. Res. (m/s)
n4095	12	1.4	3000	0.16	0.094
n511	12	0.17	3000	0.16	0.75
n63	12	0.021	3000	0.16	6.1
CW	8,10,12, 14,16	-	-	-	0.1-0.2 (/s)
Sweep	8-16	0.016s sweep each second	8000	0.08	-

The bandwidths of trial signals were selected to approximately match the ±3dB transmit sensitivity of the Chelsea Technologies CTG052 transmitter that was utilised for all signals excepting the low-frequency test signal (F_o = 545Hz).

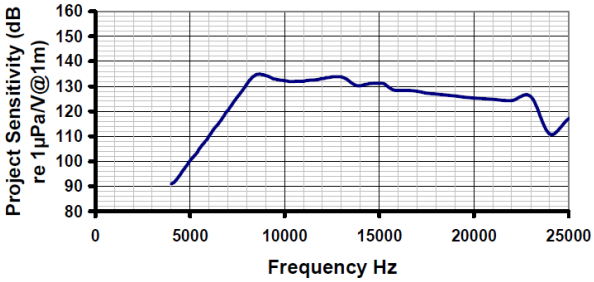

Figure 5. Transmitter sensitivity

For the medium depth trial the duration of the communication signals was much shorter, ranging from 1-3s. The low-frequency signal duration was around 70s for each transmission.

Table 2. Medium depth trial test signals

Carrier F_o (Hz)	Sequence repeat period, T (s)	Bandwidth B (Hz)	Delay Res. (ms)	Dopp. Res. (m/s)
13750	0.032	7300	0.07	3.5
11250	0.051	3800	0.13	2.7
545	2.7	105	4.75	1.05

Doppler and delay resolution

The delay resolution $\boldsymbol{\delta_t}$ of multi-path arrivals is determined by the signal bandwidth $\boldsymbol{B}$ as per Equation (1), where $\boldsymbol{B}$ is the chipping rate for an PN sequence signal, or the inverse of the sweep interval for a repeated frequency sweep.

$$\boldsymbol{\delta_t = \frac{1}{2B}} \quad (1)$$

In practice signal bandwidth is guided by the optimal transmit frequency range of the transmitter. The test signal bandwidths and associated delay resolutions are detailed in Tables 1 and 2.

It is helpful if the symbol duration, i.e. the PN sequence or sweep repetition interval, is longer than the detectable channel delay-spread to ensure that periodic signal correlation maxima are distinct from delay correlation maxima.

The Doppler shift in the receive signal may be computed for each signal repeat interval by cross-correlating the receive signal with replicas of the transmit signal resampled according to the Doppler velocity scanning range of interest.

The Doppler velocity resolution $\boldsymbol{\delta_v}$ depends on the signal repeat interval $\boldsymbol{T}$ (or sampled signal duration for a CW) and the signal carrier frequency F_o as per equation (2) where $\boldsymbol{c}$ is the speed of sound.

$$\boldsymbol{\delta_v = \frac{c}{F_o T}} \quad (2)$$

To explore the Doppler imparted to arrivals at discrete delays requires a signal with sufficient length to achieve satisfactory Doppler resolution, and also sufficiently fine delay resolution to enable the Doppler to be resolved at specific delays. In theory longer PN sequences achieve both these requirements. In practice, as the PN sequence length is increased the correlation gain tends to become degraded by variations in Doppler at timescales shorter than the sequence period.

The test signal Doppler resolutions are detailed in Tables 1 and 2.

An example Doppler-Delay ambiguity function is illustrated in Figure 6 for a 1.4s long n=4095 PN sequence modulated by a 12 kHz CW carrier. The ambiguity function is important to the interpretation of Doppler lobes in the correlation output which can be artifacts of the probe signal.

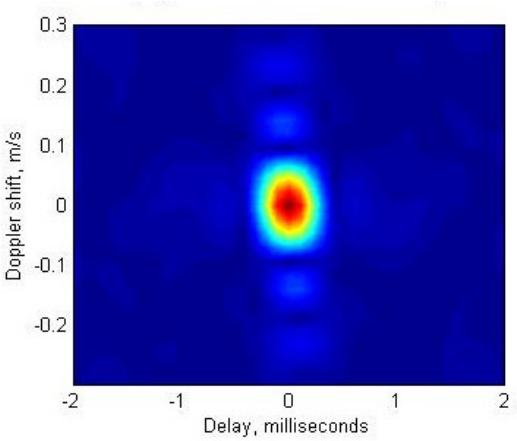

Figure 6 Ambiguity function for 1.4s N=4095 PN sequence

SHALLOW CHANNEL DELAY STRUCTURE

The arrival delay structure for an idealised ocean waveguide with specular surface and bottom reflections is illustrated in Figure 7 and Figure 8 to assist with the interpretation of the measured shallow channel delay structure. (The direct path is omitted from Figure 8).

It may be noted that at increasing ranges the time separation between delays becomes less than the delay resolution of test signals listed in Table 1.

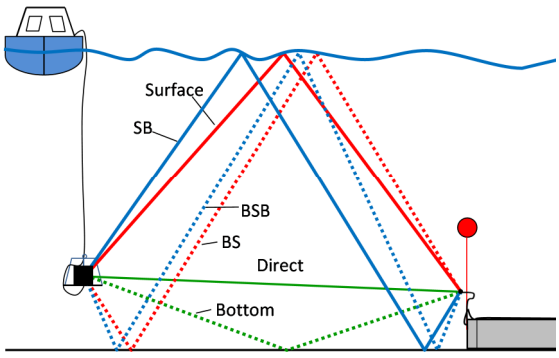

Figure 7. Low order reflected paths

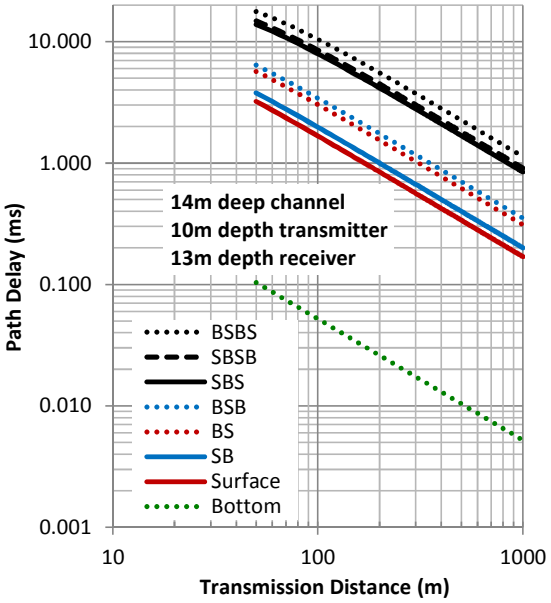

Figure 8. Idealised delay structure relative to the direct path - shallow channel

Shallow channel sea conditions

The water column was well mixed during testing with the sound speed ranging almost linearly from 1537m/s at the surface to 1536m/s at the bottom. Later in the day the sound speed of the top 1m increased by 1m/s however this does not pertain to the data presented here.

Wind conditions were light to still, with low swell and sea conditions reported at 15 minute intervals from the nearby Cottesloe Directional Wave Rider Buoy (DWRB) as summarised in Table 3.

Table 3. Wave height data for presented results

Wave type	Significant height, H_s	Wave period, T_m	Wave direction origin
Swell	0.4m	13-14s	240°-290°
Sea	0.25m	3s	180°-230°

Experimental delay results – shallow 100m range

Figures 9 to 12 show the experimental delay structure over a transmission distance of approximately 100m obtained utilising repeated PN sequence lengths ranging from 1.4 seconds to 21 milliseconds, and a 16 millisecond frequency sweep repeated at 1 second intervals. The four signal types were sampled sequentially within a 270s period while the vessel drifted and the transmission range varied from 126m to 92m.

Referring to Figure 8 the first arrival represents the combined direct and bottom-reflected path, with the second group of arrivals extending between 1ms and 3ms corresponding to Surface, BS, SB and BSB reflected paths. The next group of arrivals are apparent between 7ms and 10ms.

It may be seen that the increased transient response associated with reduced PN sequence length comes at the cost of reduced signal-to-noise ratio.

The short frequency sweeps utilised in Figure 12 offer improved time resolution and could have been repeated at a much higher rate (e.g. 20 times per second) to reveal finer structure in time.

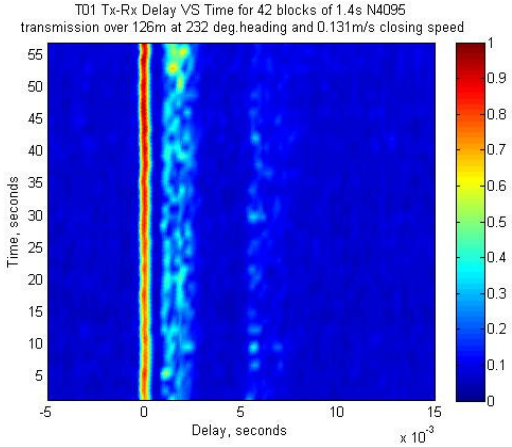

Figure 9. Channel correlation response vs delay and time – 1.4s PN sequence @ 126m

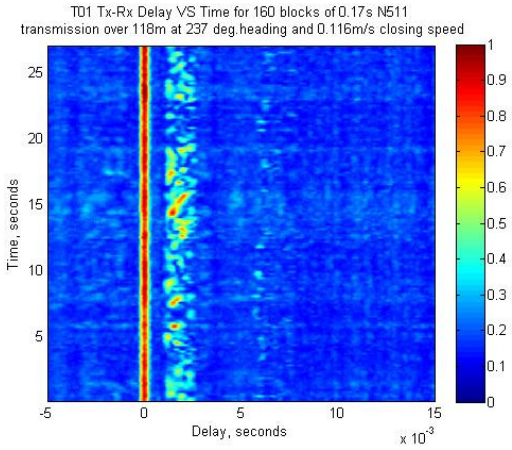

Figure 10. Channel correlation response vs delay and time – 0.17s PN sequence @ 118m

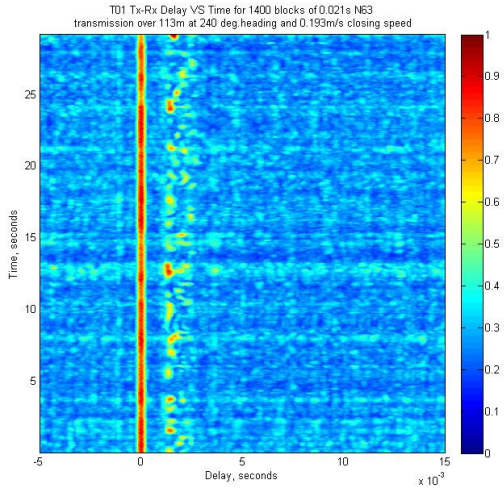

Figure 11. Channel correlation response vs delay and time – 21ms PN sequence @ 113m

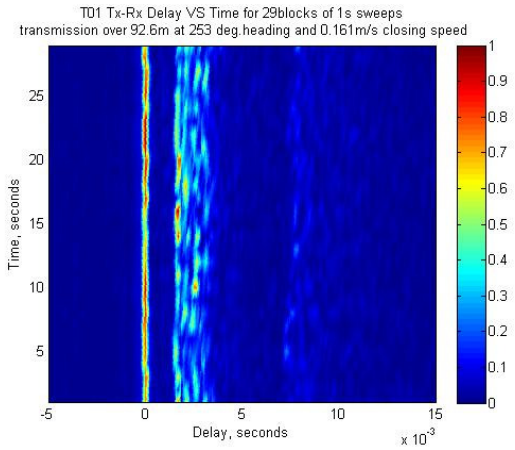

Figure 12. Channel correlation response vs delay and time – 16ms sweeps at 1s interval

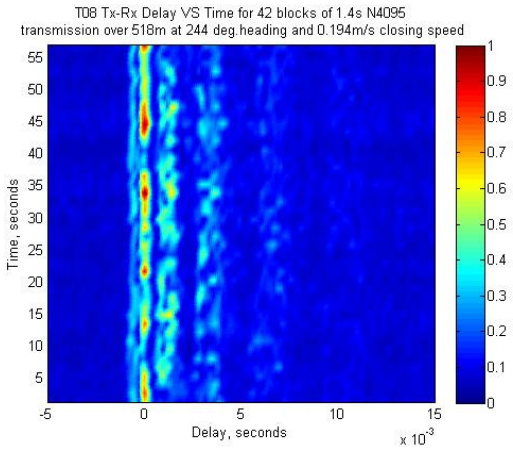

Figure 13. Channel correlation response vs delay and time – 1.4s PN sequence @ 518m

Experimental delay results – shallow 500m range

At 500m range (Figures 13 to 15) the contracting of the delay spread is aparent with two additional bands of higher order multiple reflections evident compared with the 100m range results.

The results at this range are notable as the first correlation maximum is consistently suppressed relative to the second. (It should be noted that the alignment of the second correlation with zero delay in Figures 13 and 14 reflects the alignment algorithm in these plots only, which references relative to the stronger second delay.)

The path difference of the direct and bottom bounce paths is theoretically around an eighth of a wavelength, accounting for the attenuated first correlation delay maxima, with the surface bounce arrival combining intermittently with the BS arrival to produce the highest signal correlation.

With compressed delay structure, the periodic effect of swell (recorded T_m = 13s to 14s) on the multipath correlation output is apparent in Figures 13 to 15. The nulls in correlation output that extend across all delays simultaneously are attributable to Doppler variations at a time-scale shorter than the sequence period. Nulls in correlation output that are confined to some but not all delays could be the result of either Doppler degredation of the correlation, or transient destructive interference effects of close-spaced multi-path.

For the extraction of delay information only it may be seen that when using a simple detector, sweep signals such as utilised for Figure 15 are a superior probe signal due to their Doppler insensitivity.

The advantage of coded signals for exploring channel delay structure is the ability of these signals to provide simultaneous information about the delay and Doppler characteristics of the channel.

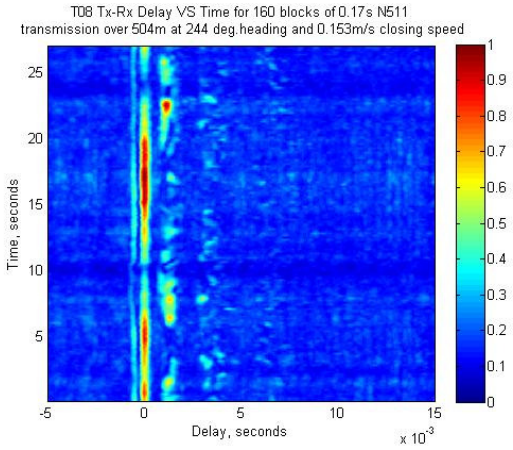

Figure 14. Channel correlation response vs delay and time – 0.17s PN sequence @ 504m

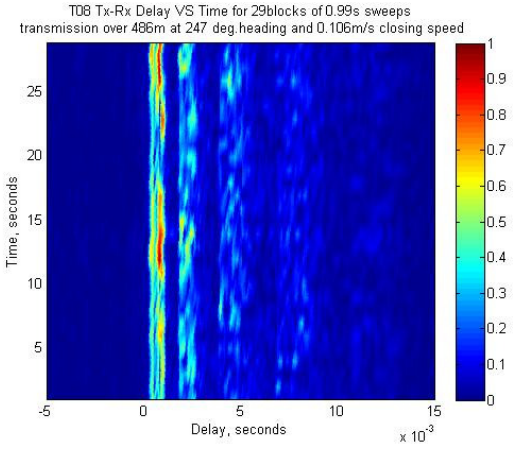

Figure 15. Channel correlation response vs delay and time – 16ms sweeps at 1s interval

Experimental delay results – shallow 1000m range

At 1000m range the relative phases of the direct, surface (~2λ delay) and bottom bounce (~0.05λ delay) constructively combine to produce a stable and strong first correlation peak. The correlation output is still modulated at an interval matching the swell period, however the minimum SNR remains relatively high as illustrated in Figure 16 and Figure 17.

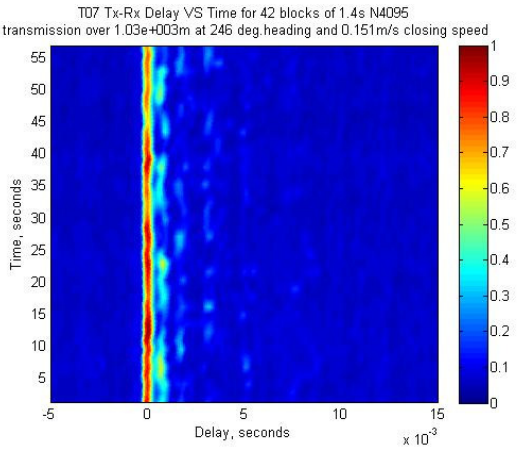

Figure 16. Channel correlation response vs delay and time – 1.4s PN sequence @ 1030m

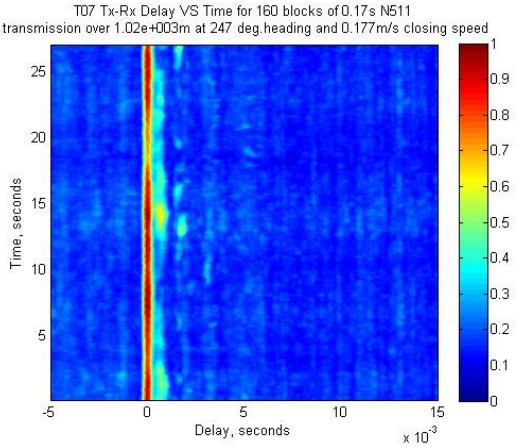

Figure 17. Channel correlation response vs delay and time – 0.17s PN sequence @ 1020m

Doppler effects – shallow channel

The net Doppler of the channel and transmitter movement has been examined for the 1.4s n=4095 PN sequence for which the Doppler resolution is 0.09m/s. Results over a 60 second period representing the maximum Doppler over all delays are presented in Figure 18 for 126m transmission range and 0.13m/s average closing speed, and Figure 19 for 1030m range and 0.15m/s average closing speed.

The results illustrate an oscillatory cycle that matches the swell period, representing the influence of swell orbital motion on the vessel and/or suspended transmitter. As the correlation maximum usually relates to the direct path, variation in path length associated with the small vertical swell displacement is not a significant factor. The average Doppler is consistent with the average transmitter-receiver closing speed that has been determined from the GPS records.

Further analysis is underway at the time of writing to examine the net Doppler at specific delays, and to separate Doppler imparted by the transmitter movement from that attributable to the channel. This analysis will be assisted by the detailed heave, pitch and roll records for the vessel, and the transmitter pressure logger record.

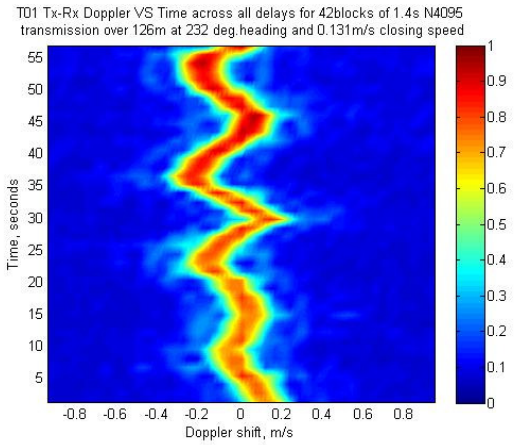

Figure 18. Channel correlation response vs Doppler and time – 1.4s PN sequence @ 126m

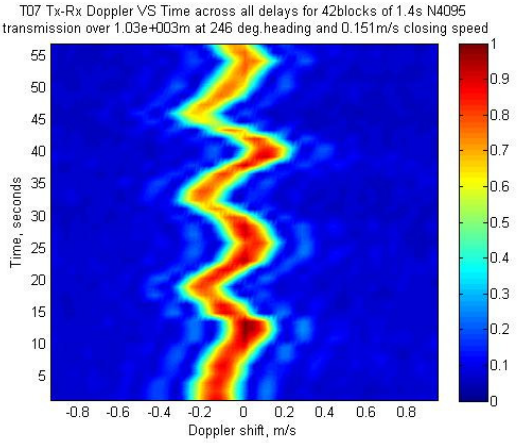

Figure 19. Channel correlation response vs Doppler and time – 1.4s PN sequence @ 1030m

MEDIUM DEPTH CHANNEL TRIAL

Wave conditions

Wave conditions during the L3-Nautronix instrument deployment trial were significantly higher than for the shallow-water trial and with shorter mean swell periods.

The wave conditions reported at 30 minute intervals from the nearby Rottnest Island DWRB are summarised in Table 4.

Table 4. Wave height data for presented results

Wave type	Significant height, H_s	Wave period, T_m	Wave direction origin
Swell	2.5–2.8m	9-9.5s	253°-262°
Sea	1.3-1.4m	4.8-4.9s	136°-243°

The CTD cast results indicated that water column was well mixed during testing with the sound speed ranging almost linearly from 1531m/s at the surface to 1532m/s at the bottom.

Idealised delay structure

The arrival delay structure for an idealised ocean waveguide with specular surface and bottom reflections is illustrated in Figure 20 for the same qualitative transmit-receive arrangement as shown in Figure 7.

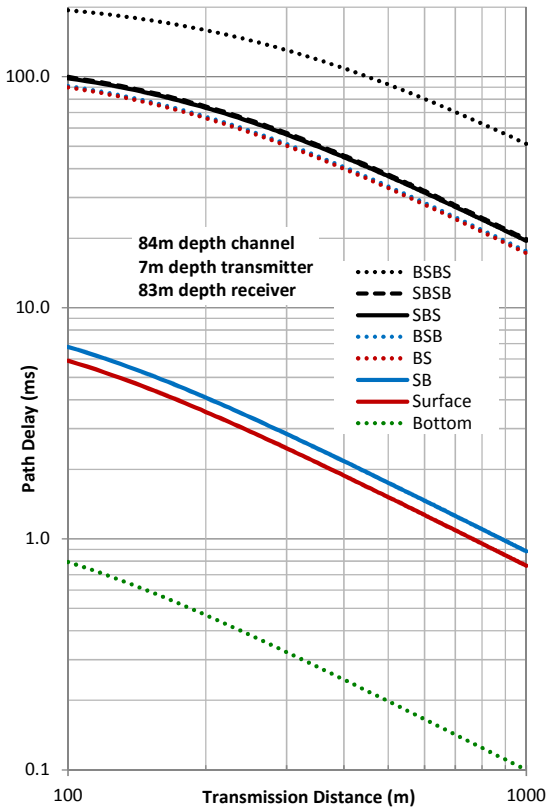

Figure 20. Idealised delay structure relative to the direct path - medium depth channel

Referring to Table 2, the Doppler sensitivity of the transmit signals utilised in the medium depth trial was low (reflecting their real-world reliability and utility). Accordingly, results are presented for the experimental channel delay structure only.

Experimental delay results – medium depth

Analysis of the delay structure revealed by the short sequence L3-Nautronix communication signals is currently in progress (Note: This analysis is independent of L3-Nautronix and unrelated to the L3-Nautronix system associated with the sampled communication signals).

A short 0.5s sample of the 0.051s sequence channel response is shown in Figure 21 to illustrate the relatively fine delay resolution that is achievable at a distance of 1040m. The bottom reflected path at around 0.2ms is faintly distinguishable from the direct path. Surface and BS reflected paths are evident at approximately 0.8ms and 1mS delay.

The fine resolution structure evident from the short-sequence (51ms) signal in Figure 21 makes an interesting contrast with the much larger scale delay structure that is revealed by the much longer 2.7s low-frequency sequence in Figure 22. The commencement of the signals in Figures 21 and 22 are coincident in time.

The delay resolution of the 2.7s signal in Figure 22 cannot separate the direct, surface, bottom, and BS arrivals, with phase interference producing a consistently weak first correlation peak, in contrast to Figure 21.

The long-sequence results displayed in Figure 22 and Figure 23 further illustrate the sensitivity of the first correlation peak to separation distance due to destructive interference of the first few arrivals.

The advantage of the 2.7s sequence is its ability to reveal larger scale arrival structure at around 20ms (comprising SB, BSB,SBS,SBSB reflections), at 50-60ms (comprising BSBS and higher order reflections) and higher order reflections at around 120ms. These larger delays are difficult to illucidate with a short sequence interval (e.g. 51ms) that is comparable to the channel delay.

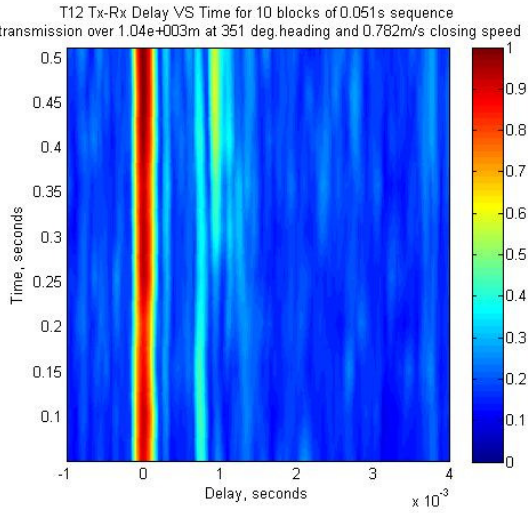

Figure 21. Channel correlation response vs delay and time – 51ms sequence @ 1040m

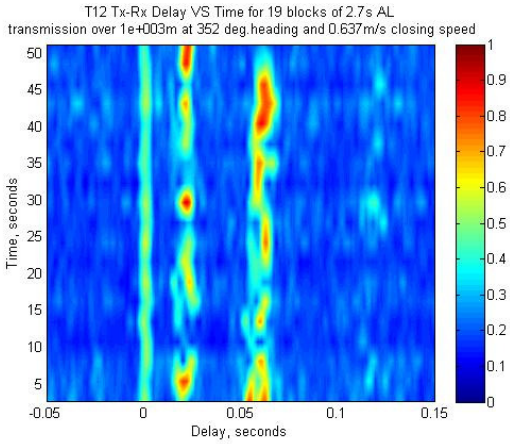

Figure 22. Channel correlation response vs delay and time – 2.7s sequence @ 1000m

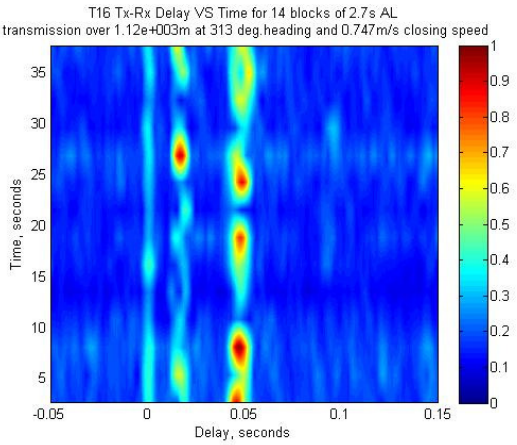

Figure 23. Channel correlation response vs delay and time – 2.7s sequence @ 1120m

The long-sequence result from 314m transmission illustrated in Figure 24 is notable for its absence of apparent delay structure. The combination of steep surface reflection angles in 84m water depth and long sequence length has resulted in no detectable correlation from paths involving surface reflections due to Doppler degradation of the correlation.

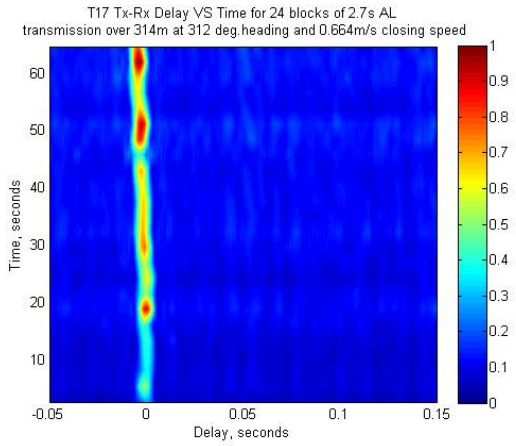

Figure 24. Channel correlation response vs delay and time – 2.7s sequence @ 314m

FURTHER INVESTIGATIONS

Further work is being undertaken to separate the Doppler contribution of transmitter movement from that associated with the channel, and to quantify the imparted Doppler and correlation intervals of surface reflected arrivals.

The second channel of receiver data will be further analysed to explore the vertical correlation of the sound fields and the benefits of spatial diversity in receiver designs.

Analysis of the medium depth delay structure is continuing utilising the more complex time-varying transmit sequences that were utilised for this trial.

The resulting transient channel characterisations are being used to guide the development of a dynamic channel simulator capable of simulating signal distortion at realistic and significant time scales.

ACKNOWLEDGEMENTS

This work was supported under the Australian Research Council's Discovery Projects funding scheme (project number DP110100736) and by L3-Communications Nautronix Ltd.

REFERENCES

Eggen, T. H. 2001. Communication over Doppler spread channels - II: Receiver characterization and practical results. *IEEE journal of oceanic engineering,* 26**,** 612-621.

Freitag, L., Stojanovic, M., Singh, S. & Johnson, M. 2001. Analysis of channel effects on direct-sequence and frequency-hopped spread-spectrum acoustic communication. *IEEE journal of oceanic engineering,* 26**,** 586-593.

Karasalo, I. Year. Modelling of Turbo-coded Acoustic Communication in Realistic Underwater Environments. *In:* 4th International Conference and Exhibition on "Underwater Acoustic Measurements: Technologies & Results", 20-24 June 2011 2011. 1089-1094.

Porter, M. B. 2011. The BELLHOP Manual and Users Guide - *preliminary draft*. HLS Research, La Jolla, CA, USA.

Siderius, M., Porter, M. B., Hursky, P. & McDonald, V. 2007. Effects of ocean thermocline variability on noncoherent underwater acoustic communications. *The Journal of the Acoustical Society of America,* 121**,** 1895-1908.

Socheleau, F.-X., Passerieux, J.-M. & Laot, C. 2011. Acoustic Modems Performance Assessment via Stochastic Replay of a At-sea Recorded Underwater Acoustic Communication Channels. *4th International Conference and Exhibition on "underwater Acoustic Measurements: Technologies & Results".*

Stojanovic, M. & Preisig, J. C. 2009. Underwater acoustic communication channels: propagation models and statistical characterization.(Underwater Wireless Communications)(Report). *IEEE communications magazine,* 47.

van Walree, P. A., Jenserud, T. & Otnes, R. 2010. Stretched-exponential Doppler spectra in underwater acoustic communication channels. *The Journal of the Acoustical Society of America,* 128**,** EL329-EL334.

van Walree, P. A., Jenserud, T. & Smedsrud, M. 2008. A Discrete-Time Channel Simulator Driven by Measured Scattering Functions. *IEEE journal on selected areas in communications,* 26**,** 1628-1637.